Stem Cell Reports
Report

ISSCR

OPEN ACCESS

Directed Differentiation of Human Pluripotent Stem Cells to Microglia

Panagiotis Douvaras,[1,*] Bruce Sun,[1] Minghui Wang,[2] Ilya Kruglikov,[1] Gregory Lallos,[1] Matthew Zimmer,[1] Cecile Terrenoire,[1] Bin Zhang,[2] Sam Gandy,[3] Eric Schadt,[2] Donald O. Freytes,[4] Scott Noggle,[1,5] and Valentina Fossati[1,5]

[1]The New York Stem Cell Foundation Research Institute, New York, NY 10019, USA
[2]Department of Genetics and Genomic Sciences, Icahn Institute for Genomics and Multiscale Biology
[3]Department of Neurology, Department of Psychiatry, Alzheimer's Disease Research Center
Icahn School of Medicine at Mount Sinai, New York, NY 10029, USA
[4]The Joint Department of Biomedical Engineering, North Carolina State University and University of North Carolina-Chapel Hill, Raleigh, NC 27695, USA
[5]Senior author
*Correspondence: pdouvaras@nyscf.org
http://dx.doi.org/10.1016/j.stemcr.2017.04.023

SUMMARY

Microglia, the immune cells of the brain, are crucial to proper development and maintenance of the CNS, and their involvement in numerous neurological disorders is increasingly being recognized. To improve our understanding of human microglial biology, we devised a chemically defined protocol to generate human microglia from pluripotent stem cells. Myeloid progenitors expressing CD14/CX3CR1 were generated within 30 days of differentiation from both embryonic and induced pluripotent stem cells (iPSCs). Further differentiation of the progenitors resulted in ramified microglia with highly motile processes, expressing typical microglial markers. Analyses of gene expression and cytokine release showed close similarities between iPSC-derived (iPSC-MG) and human primary microglia as well as clear distinctions from macrophages. iPSC-MG were able to phagocytose and responded to ADP by producing intracellular Ca^{2+} transients, whereas macrophages lacked such response. The differentiation protocol was highly reproducible across several pluripotent stem cell lines.

INTRODUCTION

Microglia are resident, tissue-specific macrophages that perform several critical roles in development and maintenance of the CNS (Hanisch and Kettenmann, 2007). They arise from primitive $CD45^{+}CX3CR1^{-}$ myeloid progenitors in the yolk sac that differentiate to $CD45^{+}CX3CR1^{+}$ microglial progenitors and invade the developing brain before the emergence of definitive hematopoiesis (Ginhoux et al., 2010; Kierdorf et al., 2013; Schulz et al., 2012). In the healthy adult brain with an intact blood-brain barrier, microglia persist as a self-sustained population that is not replenished by circulating bone marrow-derived cells (Ajami et al., 2007; Ginhoux et al., 2010). "Resting" microglia are highly active as their processes continuously examine the entire brain for homeostatic disruptions (Nimmerjahn et al., 2005).

Microglia phagocytose pathogens and cell debris and remove toxic molecules and protein deposits, thus attenuating inflammation and promoting tissue regeneration and repair (Fenn et al., 2012; Napoli and Neumann, 2009). During development, microglia promote migration and differentiation of neural progenitors, neurogenesis, and oligodendrogenesis, and regulate synaptogenesis and synaptic plasticity through pruning (Aarum et al., 2003; Paolicelli et al., 2011; Ueno et al., 2013). Microglia can also contribute to pathological brain inflammation and disruption of the blood-brain barrier by releasing cytokines and neurotoxic molecules (Colton and Gilbert, 1987; Luheshi et al., 2011). Dysfunctional microglia have been linked to amyotrophic lateral sclerosis and Alzheimer's disease. Chronic activation of microglial cells is a possible trigger to the progression of multiple sclerosis and Parkinson's disease (Kierdorf et al., 2013), and defective phagocytosis and synaptic pruning have been implicated in schizophrenia and autism spectrum disorders (Ransohoff, 2016).

Although most of our knowledge regarding microglia derives from rodent studies, there are major interspecies differences, such as proliferation rate, adhesive properties, and expression of critical receptors (Smith and Dragunow, 2014). The analysis of primary human microglia is severely limited by tissue availability, especially from healthy individuals.

We developed a robust, reproducible protocol that generates microglia from human pluripotent stem cells (PSCs) in chemically defined conditions, by mimicking embryonic development. Human induced PSC (iPSC)-derived microglia (iPSC-MG) are similar by morphology, gene expression, and cytokine release profile to human primary microglia and are distinct from other tissue macrophages. Furthermore, they are able to phagocytose and generate intracellular Ca^{2+} transients in response to ADP.

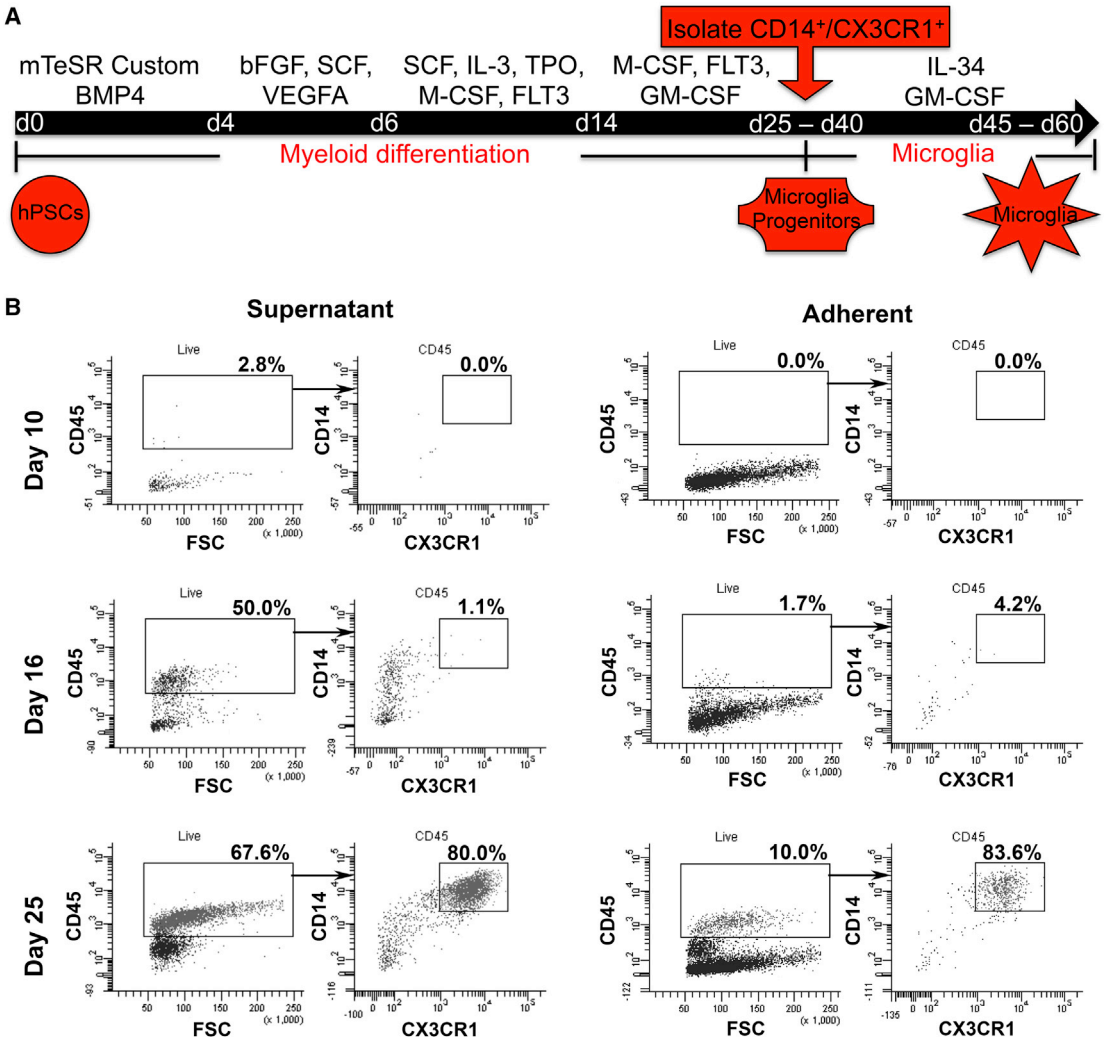

Figure 1. PSC Differentiate to Microglia through Myeloid Progenitors

(A) Diagram depicting the major steps of the microglial differentiation protocol.

(B) Kinetics of CD45, CX3CR1, and CD14 expression between day 10 and day 25 in the adherent and supernatant fractions.

See also Figure S1.

RESULTS

Differentiation of Human PSCs to Myeloid Progenitors

As microglial cells arise from myeloid progenitors in the yolk sac during development, we established a serum- and feeder-free protocol to differentiate human PSCs toward the myeloid lineage (Figure 1A). Building upon previous studies (Yanagimachi et al., 2013), we induced primitive streak-like cells through bone morphogenetic protein 4 (BMP4) signaling to obtain $KDR^+CD235a^+$ primitive hemangioblasts (Sturgeon et al., 2014) (Figure S1A). $CD45^+CX3CR1^-$ microglial progenitors appeared in the supernatant by day 16, while CX3CR1 was upregulated between days 20 and 25. In contrast, the adherent population contained only a small fraction of $CD45^+CX3CR1^+$ progenitors. Interestingly, CD14 was upregulated in a subset of $CD45^+$ cells around day 16, before the appearance of CX3CR1 (Figure 1B). Between days 25 and 50, 82% ± 5% of the $CD14^+$ cells co-expressed CX3CR1. The protocol's efficiency to generate microglial progenitors, based on CD14 expression, was 68% ± 4% across 16 lines (Figure S1D). Microglial progenitors were continuously generated in the supernatant for up to 1 month and were isolated every week with an average yield of $224 \pm 42 \times 10^3$ cells per isolation, per 100×10^3 PSCs plated. Microglial progenitors were isolated either via fluorescence-activated cell sorting (FACS) (Figures S1B and S1C) or magnetic bead separation for further differentiation or long-term storage. Thawed

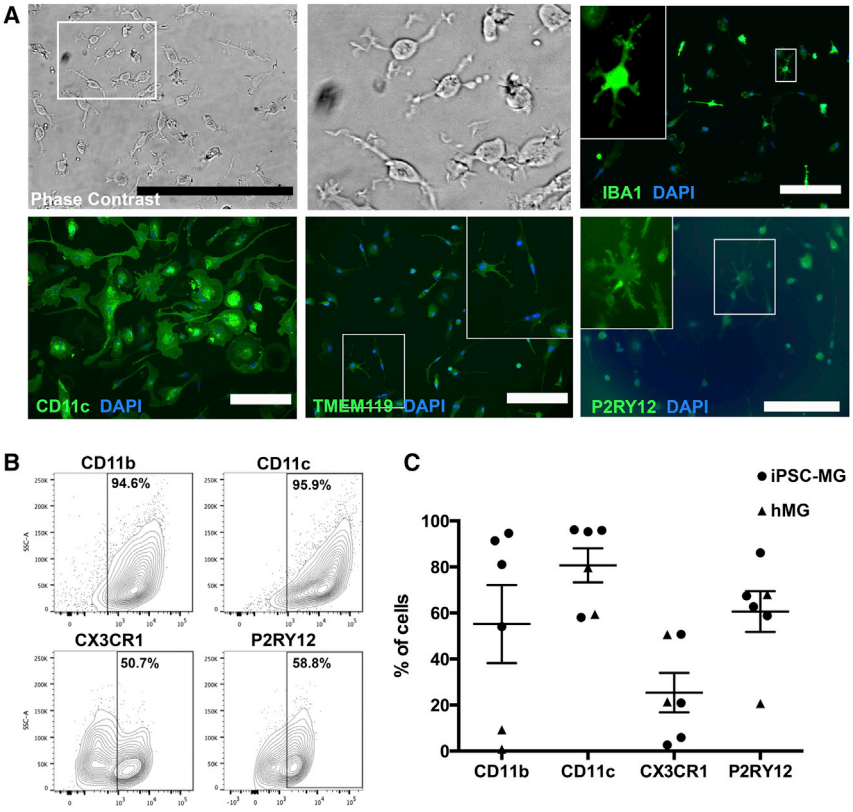

Figure 2. Characterization of iPSC-MG

(A) Panel of representative images of iPSC-MG in phase contrast and after immunofluorescent labeling for IBA1, CD11c, TMEM119, and P2RY12. White boxes indicate the areas of the magnified insets. Scale bars, 50 μm (phase contrast) and 200 μm (all other images).

(B) Representative flow-cytometry plots for typical microglial surface antigens in iPSC-MG.

(C) Dot plot showing the percentage of total cells expressing the microglial surface antigens shown in (B) across four independent iPSC-MG (depicted as circles) and two hMG samples (depicted as triangles). Error bars denote mean ± SEM.

See also Movie S1 and Figure S2 for characterization of hMG.

progenitors retained their differentiation capacity, with a post-thaw viability of 57% ± 5%.

iPSC-MG Express Typical Microglial Markers and Show Highly Motile Processes

Interleukin-34 (IL-34) and granulocyte macrophage colony-stimulating factor (GM-CSF) stimulation (Ohgidani et al., 2014) of plated microglial progenitors resulted in iPSC-MG, extending highly motile processes, constantly scanning the microenvironment (Movie S1), similarly to microglia in vivo (Davalos et al., 2005; Nimmerjahn, 2012). iPSC-MG expressed known markers such as IBA1, CD11c, TMEM119, P2RY12, CD11b, and CX3CR1 (Figures 2A–2C). Fetal human primary microglia (hMG) were used for comparison (Figure S2).

iPSC-MG Resemble Human Primary Microglia by Gene Expression

To further support the microglial identity of iPSC-MG, we performed whole-transcriptome analysis with next-generation deep RNA sequencing (RNA-seq). iPSC-MG from six unrelated healthy donors were compared with peripheral blood-derived macrophages (PB-M(−)) or polarized to M(lipopolysaccharide [LPS], interferon γ [IFNγ]), M(IL-4,IL-13), and M(IL-10), primary human hepatic macrophages (hhM), and primary human microglia cultured in serum-containing medium supplied by the provider (hMG) or in our serum-free medium (hMG-SF). We obtained high-quality reads (mean Phred quality score >38.4) and 86.2% mapped to the human genome; 18,516 genes were considered expressed and used for analysis.

iPSC-MG, hMG, and hMG-SF clustered together in a hierarchical cluster analysis using all the expressed genes showing a high degree of similarity (Spearman's correlation coefficient 0.901–0.997) and were distinct from all macrophage subtypes (Figure 3A). When we included data obtained from an independent study (Zhang et al., 2016) that isolated primary $CD45^+$ cells from human brain extracts (termed "Myeloid" in Figure 3B), iPSC-MG samples clustered together with the "Myeloid" samples, while PB-M created a distinct cluster and hhM clustered separately, appearing the most dissimilar.

Three recent studies (Bennett et al., 2016; Butovsky et al., 2014; Hickman et al., 2013) provided datasets with unique genes expressed in microglia from primary rodent cells. We selected genes that were identified in at least two of these studies and assessed their expression in our samples (Table S1). Of the 31 selected genes, 29 were expressed (at least 1 cpm) by hMG and 28 by iPSC-MG. Overall, their expression was comparable with the exception of *P2RY13*

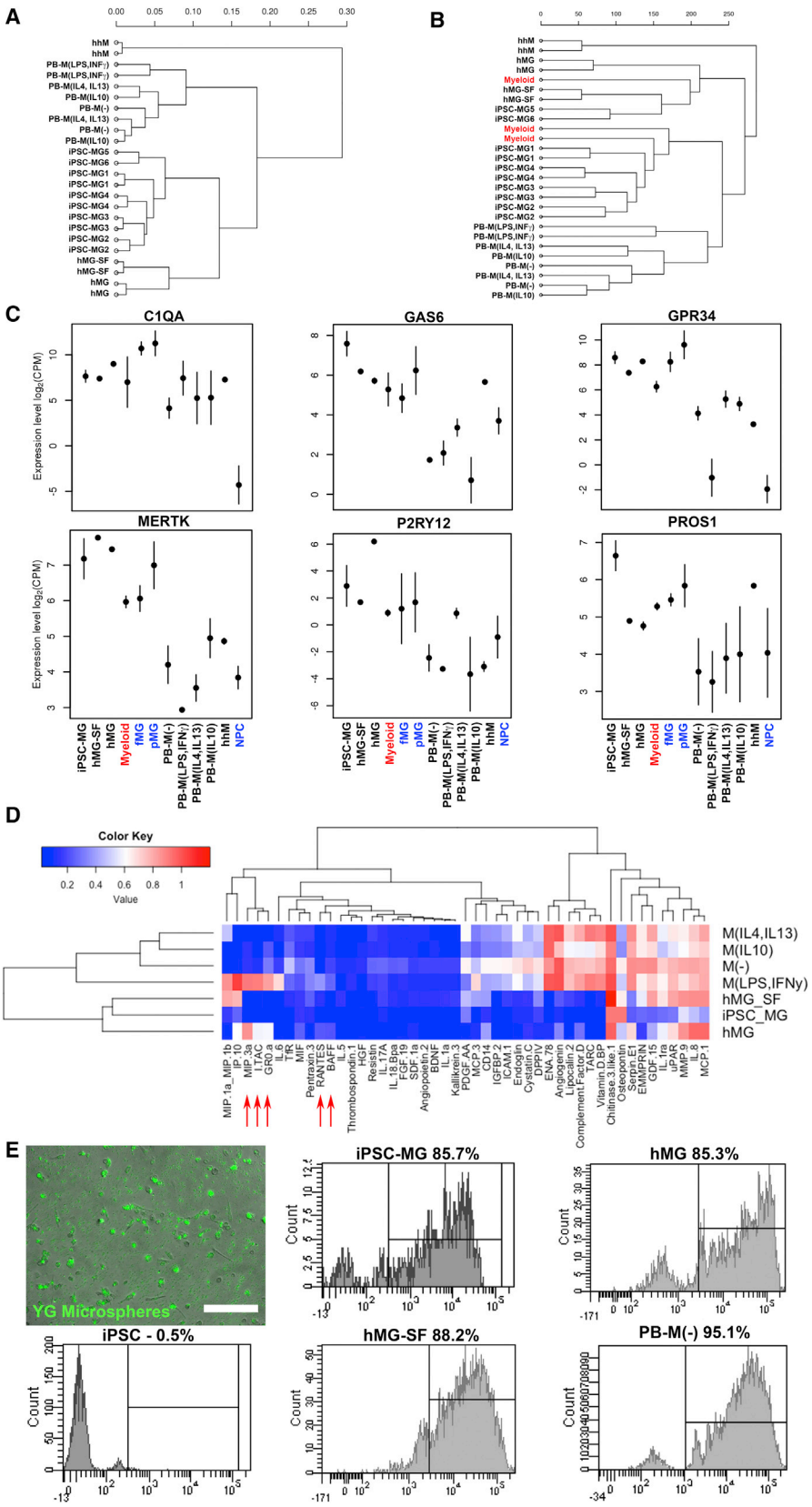

(legend on next page)

(2.6-fold lower in iPSC-MG) and *CYSLTR1* (3.8-fold lower in hMG). Moreover, *LIPH* had very low expression in all human cell types, while hMG showed low expression of *CX3CR1*, and iPSC-MG low expression of *TMEM119* and *LAG3*. However, CX3CR1 and TMEM119 proteins were detected by FACS and immunofluorescent staining, respectively.

Comparison with hhM and PB-M(−) highlighted 11 genes that were consistently higher in both iPSC-MG and hMG (shown in red in Table S1).

Butovsky et al. proposed six genes, namely *C1QA*, *GAS6*, *GPR34*, *MERTK*, *P2RY12*, and *PROS1*, as unique signature in human primary microglia. Indeed, their high expression was consistent among all our microglial samples (iPSC-MG, hMG, hMG-SF) as well as in human microglial samples from two independent studies (Muffat et al., 2016; Zhang et al., 2016) (Figure 3C), whereas macrophages and neural progenitor cells (NPCs) showed lower levels (t test: $p < 0.05$ for microglia versus macrophages or NPCs in all six genes).

Cytokine Profiles of Human iPSC-Derived and Primary Microglia Are Similar, but Differ from Peripheral Blood-Derived Macrophages

We analyzed the proteins released by iPSC-MG, hMG, hMG-SF, and PB-M, including differentially polarized macrophages (Figure 3D). Interestingly, similarities between iPSC-MG and primary microglia drastically increased when hMG were cultured in our differentiation medium (hMG-SF), as Pearson's correlation coefficient increased from $r = 0.473$ to $r = 0.824$. Of note, hMG showed upregulation of cytokines, such as RANTES, I-TAC, BAFF, GR0-a, and MIP3a, which are typically released upon inflammation, and in fact were also expressed by M(LPS,IFNγ) macrophages (red arrows in Figure 3D). Nevertheless, microglial samples clustered together and away from all PB-M subtypes.

iPSC-MG Are Functional Phagocytes

iPSC-MG, hMG, hMG-SF, PB-M, and undifferentiated iPSCs were challenged with a given amount of fluorescently labeled latex microspheres per cell. Flow-cytometry analysis showed that the majority of iPSC-MG were able to phagocytose (90% ± 6%) as were both hMG and hMG-SF. As expected, PB-M(−) macrophages were also able to engulf microspheres while undifferentiated iPSCs were not (Figure 3E).

iPSC-MG Release Intracellular Ca^{2+} in Response to ADP

The microglial signature gene *P2RY12* encodes a G_I protein-coupled receptor (Haynes et al., 2006) that responds to ADP, resulting in intracellular Ca^{2+} ($[Ca^{2+}]_i$) transients, whereas PB-M that lack P2RY12 expression do not respond to ADP (Moore et al., 2015). Thus, ADP-induced $[Ca^{2+}]_i$ transients can be used to differentiate between microglia and macrophages. When we stimulated iPSC-MG, hMG, hMG-SF, and PB-M with ADP, only microglial cells responded (Figures 4A–4C). The peak amplitude of ADP responses in iPSC-MG (Figure 4E) as well as the number of responsive cells (Figure 4F) were higher than either hMG or hMG-SF. On the contrary, none of the differentially polarized PB-M responded to ADP, but $[Ca^{2+}]_i$ transients were reliably observed upon stimulation with ATP (Figures 4D and S4).

DISCUSSION

As in vitro hematopoietic differentiation of PSCs resembles in vivo primitive hematopoiesis rather than definitive hematopoiesis (Vanhee et al., 2015), we reasoned that PSC-derived myeloid progenitors would resemble in vivo primitive yolk sac myeloid progenitors, and therefore could give rise to microglia in vitro. Stimulating PSCs with a myeloid inductive medium followed by treatment with microglia-promoting cytokines generated $KDR^+CD235a^+$ primitive hemangioblasts, which subsequently transitioned from $CD45^+CX3CR1^-$ to $CD45^+CX3CR1^+$ microglial progenitors in vitro.

To ensure robustness and reproducibility of the protocol, we tested a panel of 16 PSC lines (Table S3) including iPSCs from individuals with varying disease status, age, and sex,

Figure 3. Gene Expression, Cytokine Release Profile, and Phagocytosis of Microglia and Macrophages

(A) Hierarchical clustering dendrogram of the RNA-seq data based on global mRNA expression. Sample distances were calculated from Pearson's correlation coefficient.

(B) Dendrogram showing hierarchical clustering of our RNA-seq data and data obtained from an independent study of human primary $CD45^+$ cells in the brain ("Myeloid" samples in red, GEO: GSE73721). Analysis is based on transcriptome-wide expression.

(C) Graphs showing the expression levels of the six human microglial signature genes. Error bars are means ± SD. Colored samples correspond to data from independent studies (GEO: GSE73721 in red; GEO: GSE85839 in blue).

(D) Heatmap of the released cytokine profiles of five independent iPSC-MG runs from two lines, two independent hMG samples, and one hMG-SF sample compared with PB-M. Red arrows indicate the five proteins upregulated in hMG and M(LPS,IFNγ).

(E) Representative fluorescent image and flow-cytometry histograms showing phagocytosis of yellow-green (YG)-labeled microspheres. Scale bar, 200 μm. iPSC, undifferentiated iPSCs used as negative control.

See also Figure S3; Tables S1 and S2.

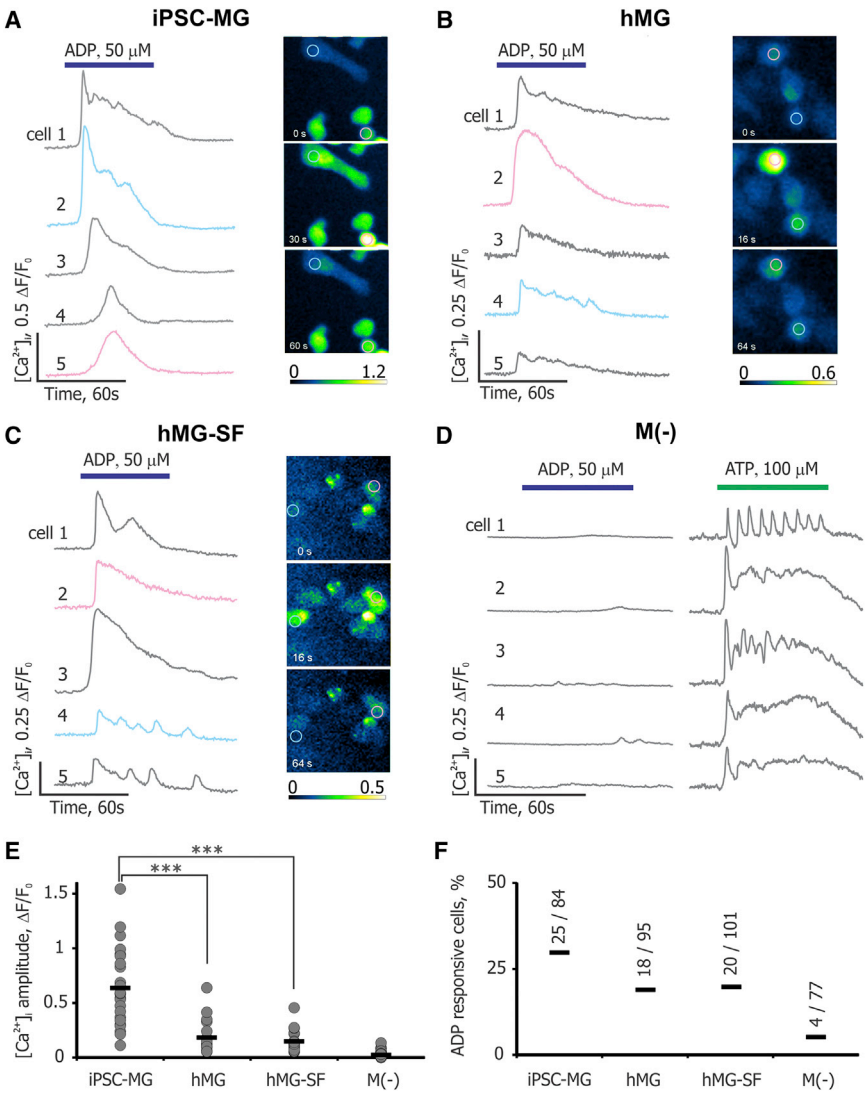

Figure 4. ADP-Evoked $[Ca^{2+}]_i$ Transients in Microglia and Macrophages

(A) Left panel shows five example traces of $[Ca^{2+}]_i$ transients following ADP application in iPSC-MG loaded with the Ca^{2+} indicator Fluo-4/AM. Right panel shows time lapse of changes in fluorescence intensity produced by ADP application. Magenta and cyan traces originate from cells indicated by same-colored regions of interest in the right panel. Bars represent duration of ADP or ATP application.

(B and C) Same data as in (A), obtained from primary human microglia (hMG) and hMG-SF correspondingly.

(D) ADP and ATP responses in PB-M(−). Note the absence of significant $[Ca^{2+}]_i$ transients in response to ADP.

(E) Statistical analysis for the amplitudes of $[Ca^{2+}]_i$ transients. Maximum amplitude of $[Ca^{2+}]_i$ transient for each responsive cell is presented as a gray dot in the corresponding category (***$p < 0.001$ by t test).

(F) Percentages of ADP-responsive cells among all different cell types analyzed. Ratios for each cell type indicate the number of responsive cells out of total number of cells analyzed. iPSC-MG data are pooled from three independent experiments.

See also Figure S4.

generated using different reprogramming strategies (e.g., mRNA/microRNA, Sendai virus). We were able to obtain microglial progenitors from all lines, with an average yield of two to three progenitors per undifferentiated PSC. The yield of progenitors varied across the lines without correlation to a specific disease, reprogramming method, or sex and age of the donor. The resulting microglia expressed typical markers, were ramified with highly motile processes, and were able to phagocytose with efficiency equivalent to that of human primary microglia.

While the identity of human microglia has not been well established, recent genome-wide studies in mouse have provided datasets to facilitate the distinction of microglia from other myeloid or CNS cell types (Bennett et al., 2016; Butovsky et al., 2014; Hickman et al., 2013). Therefore, we compared global mRNA expression of iPSC-MG with primary microglia and both peripheral blood-derived and hepatic macrophages to evaluate the proposed "signature genes" in human microglia. As obtaining all these cell types from the same individual was not feasible, we included samples with different genetic backgrounds, which may increase the "noise" of the data and possibly mask differences between cell types. However, our analyses clearly showed that iPSC-MG were clustered away from both circulating and other tissue-specific macrophages, and together with primary microglia and $CD45^+$ cells (called "myeloid"), isolated from human brains (Zhang et al., 2016). Furthermore, iPSC-MG expressed the six genes suggested as unique to human microglia (Butovsky et al., 2014) and many other genes enriched in mouse microglia (Table S1).

The cytokine profile of microglia was distinct from PB-M, independent of polarization status. iPSC-MG clustered together with hMG and tighter when hMG were cultured

in our medium (hMG-SF), probably due to the absence of serum. In vivo, microglia reside behind the blood-brain barrier, and the presence of serum components triggers their activation (Ransohoff and Perry, 2009). Indeed, hMG cultured in serum showed increased levels of inflammatory molecules such as RANTES, GR0-A, I-TAC, BAFF, and MIP3a, similarly to M(LPS,IFNγ) pro-inflammatory macrophages.

Finally, we showed that iPSC-MG express functional P2RY12 at both transcript and protein levels. This receptor distinguishes rodent and human microglia from other myeloid cells (Butovsky et al., 2014) and its activation via ADP results in $[Ca^{2+}]_i$ transients (Moore et al., 2015). All microglial samples (iPSC-MG, hMG, and hMG-SF) showed ADP-evoked $[Ca^{2+}]_i$ transients, while PB-M were unresponsive to ADP but showed $[Ca^{2+}]_i$ upon exposure to ATP, indicating that they were healthy and functional.

While this manuscript was under review, Muffat et al. (2016) published a microglial differentiation protocol, and we are providing a comparison with their RNA-seq data (Figures 3C and S3). Both approaches mimic embryonic development (derived via $CD235a^+$ yolk sac progenitors), use IL-34 as the main driver to microglial lineage commitment and maturation in chemically defined media, and generate microglia with motile processes that express typical makers and are able to perform phagocytosis. Our strategy, based on monolayer cultures instead of embryoid bodies (EBs), is comparable in efficiency but requires fewer starting PSCs. Importantly, our protocol does not require manual selection of specific EBs. We isolate microglial progenitors via FACS or magnetic beads, enabling high-throughput applications such as compound and genetic screens.

While the global expression profile of iPSC-MG strongly resembles that of human primary microglia, discrepancies were found for some microglia markers including *TMEM119*, *LAG3*, and *CX3CR1*. Surprisingly, mRNA levels of *TMEM119* were very low in iPSC-MG compared with hMG, even though the protein was detected by immunofluorescence. *TMEM119* mRNA levels in the study by Muffat et al. (2016) were variable across different iPSC lines and there was a trend for downregulation when cells were cultured in "NPC-conditioned medium." Another recent differentiation protocol (Pandya et al., 2017) describes the generation of iPSC-derived microglia from hematopoietic progenitors but requires astrocyte co-culture in the presence of serum. Under these experimental conditions, microglia differentiation is accomplished within 4 weeks with a yield comparable with both our and the Muffat protocols. Although their gene expression analysis was performed using microarrays, limiting direct comparison of expression data, *TMEM119* was also not highly expressed and not significantly different from iPSC or fetal MG expression in their dataset. On the other hand, serum exposure upregulated *TMEM119* in our hMG, suggesting that culture environment can alter expression. As studies in rodents suggest that *Tmem119* is developmentally regulated (Bennett et al., 2016), variable expression could also reflect immaturity. In addition, minimal levels of *LAG3* mRNA were detected in human primary and iPSC-derived microglia, unless they were exposed to either "NPC-conditioned medium" (in Muffat et al., 2016) or serum, despite previous studies in rodents (Butovsky et al., 2014; Hickman et al., 2013) that identified *Lag3* as a key microglial gene. As microglia are particularly sensitive to exogenous stimuli, different culture conditions are likely responsible for the subtle discrepancies in transcript levels observed between different protocols. Furthermore, microglia are known to express the chemokine receptor CX3CR1 early in development, and it was detected by flow cytometry in both hMG and iPSC-MG derived through our protocol and from Pandya et al. (2017). In contrast, mRNA was not considered expressed in human primary microglia (Muffat et al., 2016 and our study) or iPSC-derived microglia (Muffat et al., 2016) and varied in our iPSC-MG. Transcript levels of *CX3CR1* were also relatively low and variable in the Pandya et al. (2017) study despite detectable protein expression by FACS. Further work will be needed to address these discrepancies and distinguish culture-related regulation from developmental regulation of markers.

Overall, our protocol provides iPSC-MG as a new source of human microglial cells, which will complement studies in mouse models to better understand the role of microglia in health and disease. We have shown that the protocol is highly reproducible, and we anticipate that it will become a critical tool to investigate microglial dysfunction in CNS disorders. The inclusion of microglia in co-culture or three-dimensional systems, involving iPSC-derived neurons and other glial cell types, will be crucial to advance in vitro disease modeling and better recapitulate the complexity of the in vivo environment.

EXPERIMENTAL PROCEDURES

Pluripotent Stem Cell Lines

Two human embryonic stem cell lines (RUES1 and H9, both NIH approved) and 13 iPSC lines reprogrammed at New York Stem Cell Foundation upon institutional review board approvals and informed consent and one iPSC line from Dr. Ricardo Feldman were used in this study (Supplemental Experimental Procedures and Table S3). Human primary microglia and hepatic macrophages were purchased from ScienCell Research Laboratories.

Microglial Differentiation Protocol

PSC differentiation was induced with mTeSR Custom medium (STEMCELL Technologies) containing 80 ng/mL BMP4. At day 4 cells

were induced with 25 ng/mL basic fibroblast growth factor, 100 ng/mL stem cell factor (SCF), and 80 ng/mL vascular endothelial growth factor in StemPro-34 SFM (with 2 mM GutaMAX, Life Technologies). Two days later, the medium was supplemented with 50 ng/mL SCF, 50 ng/mL IL-3, 5 ng/mL thrombopoietin, 50 ng/mL macrophage CSF (M-CSF) and 50 ng/mL Flt3l, and from day 14 with 50 ng/mL M-CSF, 50 ng/mL Flt3l, and 25 ng/mL GM-CSF. Between days 25 and 50, $CD14^+$ or $CD14^+CX3CR1^+$ progenitors were isolated and plated onto tissue culture-treated dishes or Thermanox plastic coverslips (all from Thermo Fisher Scientific) in Microglial Medium (RPMI-1640 [Life Technologies] with 2 mM GlutaMAX-I, 10 ng/mL GM-CSF, and 100 ng/mL IL-34). Medium was replenished every 3–4 days for at least 2 weeks.

Other experimental procedures are described in the Supplemental Experimental Procedures.

ACCESSION NUMBERS

The accession number for the RNA-seq data reported in this paper is GEO: GSE97744.

SUPPLEMENTAL INFORMATION

Supplemental Information includes Supplemental Experimental Procedures, four figures, three tables, and one movie and can be found with this article online at http://dx.doi.org/10.1016/j.stemcr.2017.04.023.

AUTHOR CONTRIBUTIONS

P.D., D.O.F., V.F., and S.N. designed the study and reviewed the manuscript with input from S.G. and E.S., and all authors. P.D. contributed to every assay and analysis. B.S. and G.L. performed differentiation experiments, I.K. and C.T. Ca^{2+} imaging and analysis, and M.Z. flow cytometry. M.W. and B.Z. analyzed the RNA-seq data. D.O.F. analyzed the cytokine release data. P.D. and V.F. wrote the paper.

ACKNOWLEDGMENTS

We thank Dr. Isabella Pallotta and Emily Wrona for help with PB-M, and Drs. Ricardo Feldman, Aiqun Li, and Daniel Paul for the iPSC lines. This work was supported by the New York Stem Cell Foundation, the NIA/NIH grant U01AG046170 (to B.Z., M.W., E.S., S.G., and S.N.) a component of the AMP-AD Target Discovery and Preclinical Validation Project, the ORIO-13-051 grant (to D.O.F.) from the Oak Foundation, and by the 20140243 grant (to V.F.) from the Conrad N. Hilton Foundation. P.D. is an NYSCF-Druckenmiller fellow.

Received: September 1, 2016
Revised: April 20, 2017
Accepted: April 20, 2017
Published: May 18, 2017

REFERENCES

Aarum, J., Sandberg, K., Haeberlein, S.L., and Persson, M.A. (2003). Migration and differentiation of neural precursor cells can be directed by microglia. Proc. Natl. Acad. Sci. USA *100*, 15983–15988.

Ajami, B., Bennett, J.L., Krieger, C., Tetzlaff, W., and Rossi, F.M. (2007). Local self-renewal can sustain CNS microglia maintenance and function throughout adult life. Nat. Neurosci. *10*, 1538–1543.

Bennett, M.L., Bennett, F.C., Liddelow, S.A., Ajami, B., Zamanian, J.L., Fernhoff, N.B., Mulinyawe, S.B., Bohlen, C.J., Adil, A., Tucker, A., et al. (2016). New tools for studying microglia in the mouse and human CNS. Proc. Natl. Acad. Sci. USA *113*, E1738–E1746.

Butovsky, O., Jedrychowski, M.P., Moore, C.S., Cialic, R., Lanser, A.J., Gabriely, G., Koeglsperger, T., Dake, B., Wu, P.M., Doykan, C.E., et al. (2014). Identification of a unique TGF-beta-dependent molecular and functional signature in microglia. Nat. Neurosci. *17*, 131–143.

Colton, C.A., and Gilbert, D.L. (1987). Production of superoxide anions by a CNS macrophage, the microglia. FEBS Lett. *223*, 284–288.

Davalos, D., Grutzendler, J., Yang, G., Kim, J.V., Zuo, Y., Jung, S., Littman, D.R., Dustin, M.L., and Gan, W.B. (2005). ATP mediates rapid microglial response to local brain injury in vivo. Nat. Neurosci. *8*, 752–758.

Fenn, A.M., Henry, C.J., Huang, Y., Dugan, A., and Godbout, J.P. (2012). Lipopolysaccharide-induced interleukin (IL)-4 receptor-alpha expression and corresponding sensitivity to the M2 promoting effects of IL-4 are impaired in microglia of aged mice. Brain Behav. Immun. *26*, 766–777.

Ginhoux, F., Greter, M., Leboeuf, M., Nandi, S., See, P., Gokhan, S., Mehler, M.F., Conway, S.J., Ng, L.G., Stanley, E.R., et al. (2010). Fate mapping analysis reveals that adult microglia derive from primitive macrophages. Science *330*, 841–845.

Hanisch, U.K., and Kettenmann, H. (2007). Microglia: active sensor and versatile effector cells in the normal and pathologic brain. Nat. Neurosci. *10*, 1387–1394.

Haynes, S.E., Hollopeter, G., Yang, G., Kurpius, D., Dailey, M.E., Gan, W.B., and Julius, D. (2006). The P2Y12 receptor regulates microglial activation by extracellular nucleotides. Nat. Neurosci. *9*, 1512–1519.

Hickman, S.E., Kingery, N.D., Ohsumi, T.K., Borowsky, M.L., Wang, L.C., Means, T.K., and El Khoury, J. (2013). The microglial sensome revealed by direct RNA sequencing. Nat. Neurosci. *16*, 1896–1905.

Kierdorf, K., Erny, D., Goldmann, T., Sander, V., Schulz, C., Perdiguero, E.G., Wieghofer, P., Heinrich, A., Riemke, P., Holscher, C., et al. (2013). Microglia emerge from erythromyeloid precursors via Pu.1- and Irf8-dependent pathways. Nat. Neurosci. *16*, 273–280.

Luheshi, N.M., Kovacs, K.J., Lopez-Castejon, G., Brough, D., and Denes, A. (2011). Interleukin-1alpha expression precedes IL-1beta after ischemic brain injury and is localised to areas of focal neuronal loss and penumbral tissues. J. Neuroinflammation *8*, 186.

Moore, C.S., Ase, A.R., Kinsara, A., Rao, V.T., Michell-Robinson, M., Leong, S.Y., Butovsky, O., Ludwin, S.K., Seguela, P., Bar-Or, A., et al. (2015). P2Y12 expression and function in alternatively activated human microglia. Neurol. Neuroimmunol. Neuroinflamm. *2*, e80.

Muffat, J., Li, Y., Yuan, B., Mitalipova, M., Omer, A., Corcoran, S., Bakiasi, G., Tsai, L.H., Aubourg, P., Ransohoff, R.M., et al. (2016).

Efficient derivation of microglia-like cells from human pluripotent stem cells. Nat. Med. *22*, 1358–1367.

Napoli, I., and Neumann, H. (2009). Microglial clearance function in health and disease. Neuroscience *158*, 1030–1038.

Nimmerjahn, A. (2012). Two-photon imaging of microglia in the mouse cortex in vivo. Cold Spring Harb. Protoc. *2012*. http://dx.doi.org/10.1101/pdb.prot069294.

Nimmerjahn, A., Kirchhoff, F., and Helmchen, F. (2005). Resting microglial cells are highly dynamic surveillants of brain parenchyma in vivo. Science *308*, 1314–1318.

Ohgidani, M., Kato, T.A., Setoyama, D., Sagata, N., Hashimoto, R., Shigenobu, K., Yoshida, T., Hayakawa, K., Shimokawa, N., Miura, D., et al. (2014). Direct induction of ramified microglia-like cells from human monocytes: dynamic microglial dysfunction in Nasu-Hakola disease. Sci. Rep. *4*, 4957.

Pandya, H., Shen, M.J., Ichikawa, D.M., Sedlock, A.B., Choi, Y., Johnson, K.R., Kim, G., Brown, M.A., Elkahloun, A.G., Maric, D., et al. (2017). Differentiation of human and murine induced pluripotent stem cells to microglia-like cells. Nat. Neurosci. *20*, 753–759.

Paolicelli, R.C., Bolasco, G., Pagani, F., Maggi, L., Scianni, M., Panzanelli, P., Giustetto, M., Ferreira, T.A., Guiducci, E., Dumas, L., et al. (2011). Synaptic pruning by microglia is necessary for normal brain development. Science *333*, 1456–1458.

Ransohoff, R.M. (2016). How neuroinflammation contributes to neurodegeneration. Science *353*, 777–783.

Ransohoff, R.M., and Perry, V.H. (2009). Microglial physiology: unique stimuli, specialized responses. Annu. Rev. Immunol. *27*, 119–145.

Schulz, C., Gomez Perdiguero, E., Chorro, L., Szabo-Rogers, H., Cagnard, N., Kierdorf, K., Prinz, M., Wu, B., Jacobsen, S.E., Pollard, J.W., et al. (2012). A lineage of myeloid cells independent of Myb and hematopoietic stem cells. Science *336*, 86–90.

Smith, A.M., and Dragunow, M. (2014). The human side of microglia. Trends Neurosci. *37*, 125–135.

Sturgeon, C.M., Ditadi, A., Awong, G., Kennedy, M., and Keller, G. (2014). Wnt signaling controls the specification of definitive and primitive hematopoiesis from human pluripotent stem cells. Nat. Biotechnol. *32*, 554–561.

Ueno, M., Fujita, Y., Tanaka, T., Nakamura, Y., Kikuta, J., Ishii, M., and Yamashita, T. (2013). Layer V cortical neurons require microglial support for survival during postnatal development. Nat. Neurosci. *16*, 543–551.

Vanhee, S., De Mulder, K., Van Caeneghem, Y., Verstichel, G., Van Roy, N., Menten, B., Velghe, I., Philippe, J., De Bleser, D., Lambrecht, B.N., et al. (2015). In vitro human embryonic stem cell hematopoiesis mimics MYB-independent yolk sac hematopoiesis. Haematologica *100*, 157–166.

Yanagimachi, M.D., Niwa, A., Tanaka, T., Honda-Ozaki, F., Nishimoto, S., Murata, Y., Yasumi, T., Ito, J., Tomida, S., Oshima, K., et al. (2013). Robust and highly-efficient differentiation of functional monocytic cells from human pluripotent stem cells under serum- and feeder cell-free conditions. PLoS One *8*, e59243.

Zhang, Y., Sloan, S.A., Clarke, L.E., Caneda, C., Plaza, C.A., Blumenthal, P.D., Vogel, H., Steinberg, G.K., Edwards, M.S., Li, G., et al. (2016). Purification and characterization of progenitor and mature human astrocytes reveals transcriptional and functional differences with mouse. Neuron *89*, 37–53.

Stem Cell Reports, Volume *8*

Supplemental Information

Directed Differentiation of Human Pluripotent Stem Cells to Microglia

Panagiotis Douvaras, Bruce Sun, Minghui Wang, Ilya Kruglikov, Gregory Lallos, Matthew Zimmer, Cecile Terrenoire, Bin Zhang, Sam Gandy, Eric Schadt, Donald O. Freytes, Scott Noggle, and Valentina Fossati

Supplemental Information

Supplemental Data

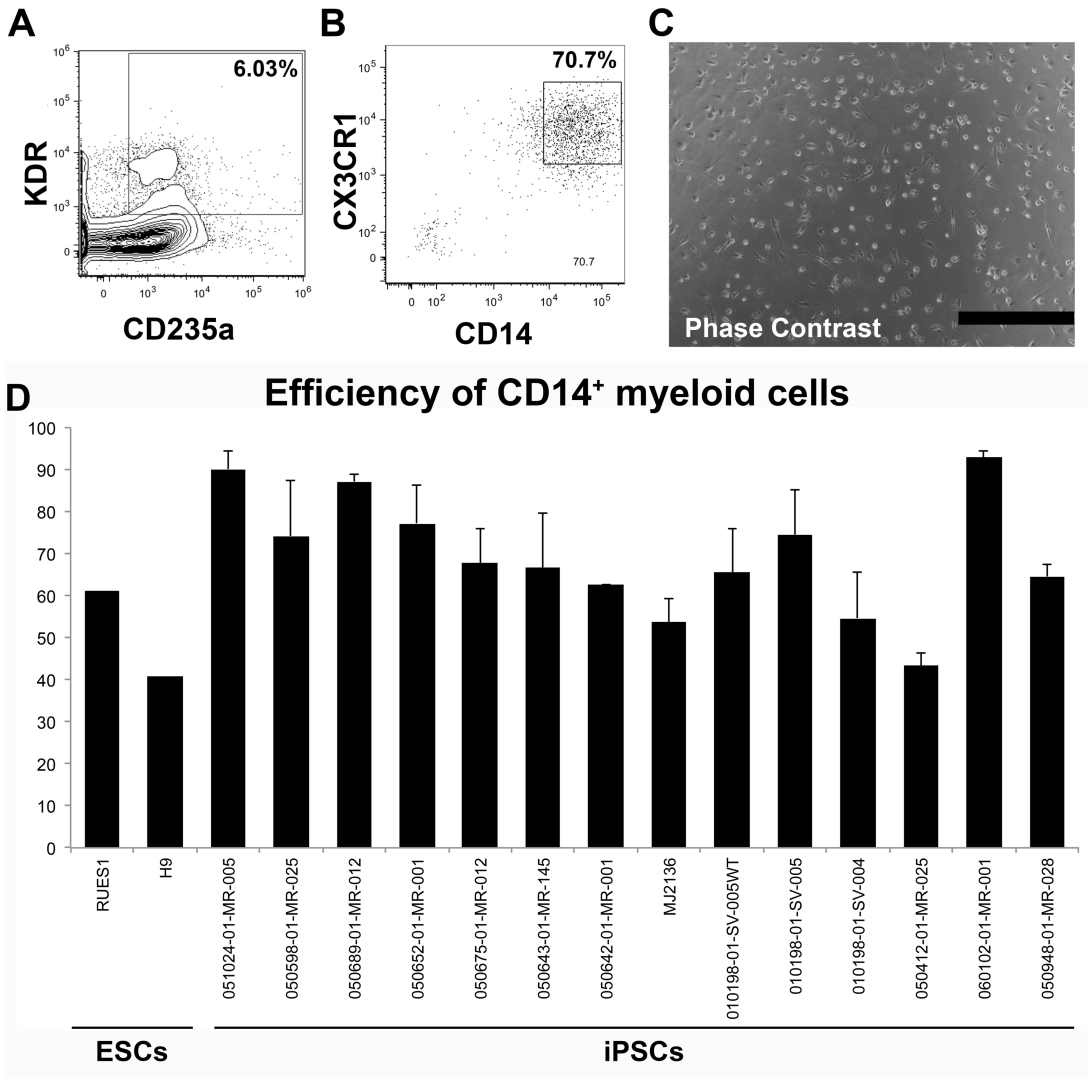

Figure S1. Microglial progenitors. Related to Figure 1. (A) Primitive hemagioblasts could be identified as $KDR^{+}CD235a^{+}$ in the adherent fraction of day 6 cultures. **(B)** Representative plot of the sorting gate used to isolate $CD14^{+}CX3CR1^{+}$ microglial progenitors via FACS between day 25 and 50 of differentiation. **(C)** Phase contrast image of plated microglial progenitors two days after isolation. Scale bar is 500µm. **(D)** Graph showing the performance of 2 ESC and 14 iPSC lines in generating $CD14^{+}$ myeloid progenitors, quantified by flow cytometry. For the iPSC lines, data were pooled from 2-7 different isolations from 1-3 independent differentiation experiments. ESCs lines are shown for comparison.

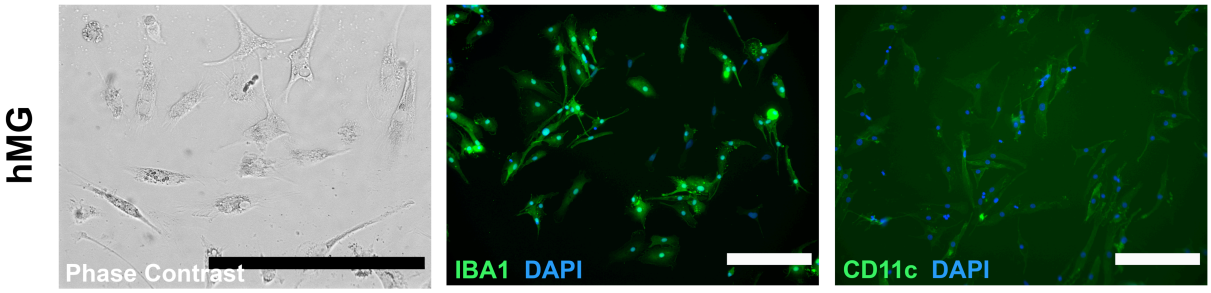

Figure S2. Characterization of human primary microglia (hMG). Related to Figure 2. Panel of representative images of hMG in phase contrast, and after immunofluorescent labeling for IBA1 and CD11c. Scale bars from left to right are 500µm, 200µm and 200µm

		iPSC-MG	hMG-SF	hhM	PB-M(-)	iPSC-MG/ hMG-SF	iPSC-MG/ hhM	iPSC-MG/ PB-M(-)
Common in all 3 studies	TREM2	10.0	8.7	4.5	8.6	1.2	2.2	1.2
	SLCO2B1	9.7	9.7	7.1	6.4	1.0	1.4	1.5
	HEXB	9.6	9.1	8.5	9.3	1.0	1.1	1.0
	GPR34	8.8	7.6	3.4	4.3	1.2	2.5	2.0
	OLFML3	3.4	5.7	6.9	1.6	0.6	0.5	2.2
	SLC2A5	2.9	4.3	3.8	6.9	0.7	0.8	0.4
	P2RY12	2.4	1.2	-3.6	-2.9	2.0	-0.7	-0.8
	P2RY13	1.1	3.0	-1.6	-1.1	0.4	-0.7	-1.0
	TMEM119	-0.5	2.7	4.7	-2.5	-0.2	-0.1	0.2
	LIPH	-4.4	-3.4	-1.7	-2.2	1.3	2.6	2.0
Butovsky & Bennett	CTSD	11.0	12.5	9.3	11.7	0.9	1.2	0.9
	TGFBR1	9.2	7.4	9.7	7.6	1.2	1.0	1.2
	ENTPD1	8.3	6.3	5.1	6.0	1.3	1.6	1.4
	IL10RA	8.2	7.0	7.6	8.5	1.2	1.1	1.0
	LAIR1	7.2	8.4	7.2	8.0	0.9	1.0	0.9
	CYSLTR1	5.6	1.4	0.7	1.7	3.8	7.6	3.3
	BLNK	4.8	4.8	0.5	2.5	1.0	9.7	2.0
	RAB3IL1	4.8	4.7	2.8	3.0	1.0	1.7	1.6
	GOLM1	4.5	3.8	6.8	3.5	1.2	0.7	1.3
	PMEPA1	4.1	3.6	4.2	2.2	1.1	1.0	1.9
	OPHN1	3.6	3.4	2.6	3.5	1.0	1.4	1.0
	CCR5	3.6	6.1	4.7	5.5	0.6	0.8	0.6
Butovsky & Hickman	F11R	8.0	7.6	6.4	8.6	1.1	1.3	0.9
	ADORA3	7.0	7.4	1.4	1.7	0.9	4.9	4.1
	SPINT1	6.9	5.2	3.0	7.8	1.3	2.3	0.9
	CCL4	5.0	6.5	8.0	1.7	0.8	0.6	2.9
	CRYBB1	3.2	3.2	1.0	-1.1	1.0	3.2	-2.9
	CX3CR1	0.8	-5.7	-1.2	-3.1	-0.1	-0.6	-0.2
	ANG	0.4	0.6	0.6	1.5	0.7	0.8	0.3
Hickman & Bennett	LAG3	-2.4	0.2	-2.0	-1.6	-11.1	1.2	1.4
	GAL3ST4	3.0	4.3	2.7	-0.8	0.7	1.1	-3.9

Table S1. Expression of murine microglial signature genes in human cells. Related to Figure 3. Normalized mean expression (log_2 transformed CPM) for 31 genes that have been identified as microglial signature genes by at least two out of three independent murine studies (Hickman et al., 2013, Butovsky et al., 2014 and Bennett et al., 2016). Genes in red are consistently higher in microglia than macrophages.

	iPSC-MG1	iPSC-MG2	iPSC-MG3	iPSC-MG4	iPSC-MG5	iPSC-MG6	hMG-SF	hMG
C1QA	9.2	8.5	9.1	9.5	7.9	7.9	8.6	10.2
GAS6	7.0	6.0	7.6	7.0	6.7	6.2	5.4	5.0
GPR34	9.2	8.5	9.1	8.9	8.2	8.0	7.6	8.5
MERTK	7.6	7.3	7.7	8.5	8.8	8.6	8.6	8.3
P2RY12	4.2	0.4	3.0	3.2	0.9	1.6	1.2	5.7
PROS1	6.2	6.4	6.8	6.8	6.0	5.7	4.7	4.5

Table S2. Expression of the six human microglial validated signature genes in the microglial samples. Related to Figure 3. Expression of the selected genes in every microglial sample from the RNAseq data. Values are $\log_2$ transformed CPM.

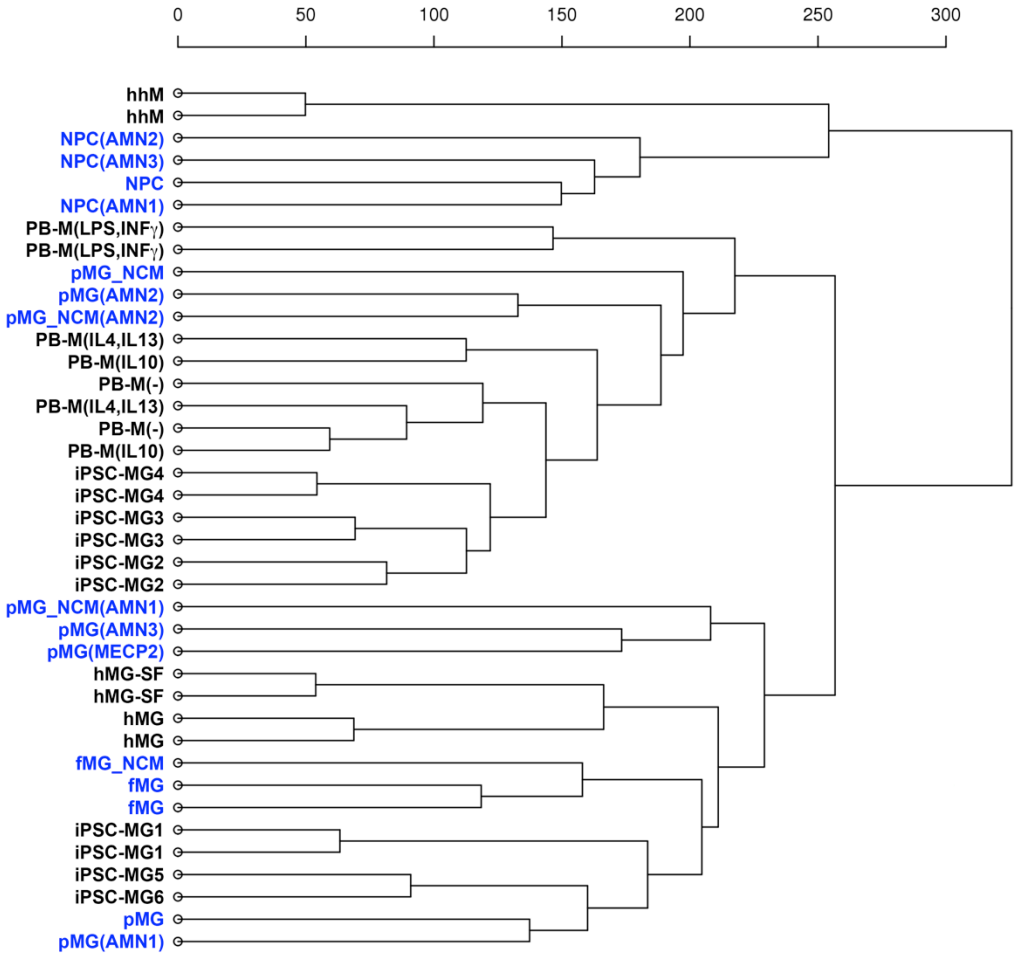

Figure S3. Comparison of RNA sequencing data to Muffat et al., 2016. Related to Figure 3. Dendrogram showing hierarchical clustering of our RNA sequencing data with data obtained from an independent study (Muffat et al., 2016) on iPSC-derived microglia (marked in blue). Analysis is based on global RNA expression after batch correction.

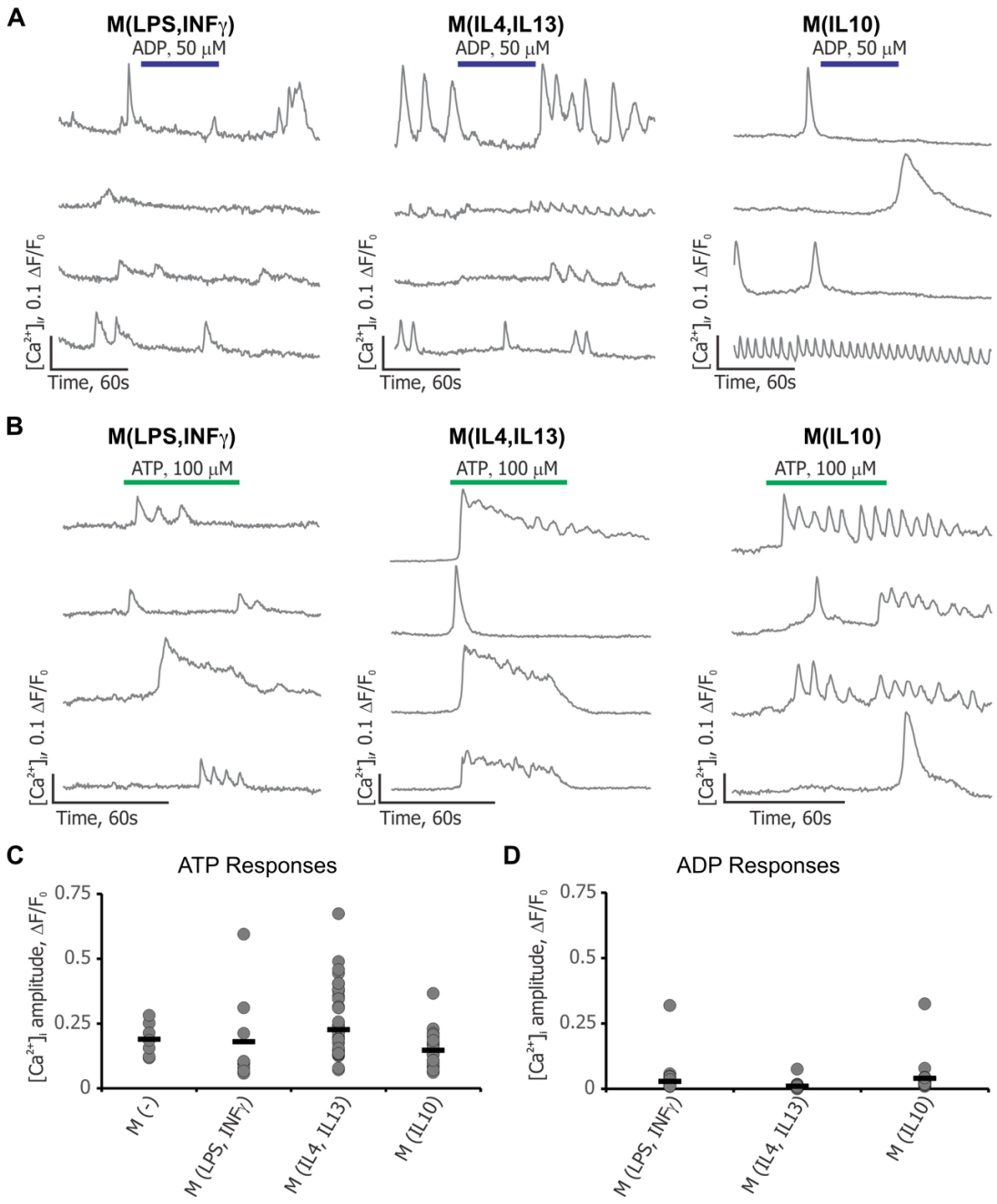

Figure S4. Intracellular Ca^{2+} transients in human peripheral blood macrophages. Related to Figure 4. Four example traces of intracellular Ca^{2+} changes during **(A)** ADP or **(B)** ATP application in macrophages polarized with (LPS,INFγ), (IL4,IL13) and (IL10). Bars represent duration of ADP (in A) or ATP (in B) application. Statistical analysis for the amplitudes of $[Ca^{2+}]_i$ transients of **(C)** ATP-responsive or **(D)** ADP-responsive macrophages. Maximum amplitude of $[Ca^{2+}]_i$ transient for each responsive cell is presented as a grey dot. The number of responsive cells is as follows: M(-) 7; M(LPS,INFγ) 9; M(IL4,IL13) 53; M(IL10) 23. Blood samples from 1-3 individuals were used to isolate monocytes that were differentiated to different macrophage subtypes.

Cell Lines	Health Status	Sex	Age	Reprogr. Method	Progenitor Efficiency	MG Markers	RNAseq	Cytokine Profiler	Phagocytosis	ADP Response	Movie
hESC RUES1	unk.	M	N/A	N/A	X$	X					
hESC H9	unk.	F	N/A	N/A	X$						
iPSC 051024-01-MR-005	w.t.	M	29	Aut. mRNA	X$	X#	X#$			X	X
iPSC 050598-01-MR-025	w.t.	M	53	Aut. mRNA	X$	X#	X#$			X	X
iPSC 050689-01-MR-012	w.t.	M	27	Aut. mRNA	X$	X#	X#$				
iPSC 050652-01-MR-001	w.t.	F	45	Aut. mRNA	X$	X		X#		X#	X
iPSC 050675-01-MR-012	w.t.	M	34	Aut. mRNA	X$		X#$				
iPSC 050643-01-MR-145	w.t.	M	25	Aut. mRNA	X$	X#	X#$	X#	X#		
iPSC 050642-01-MR-001	w.t.	M	69	Aut. mRNA	X$	X#	X#$				
iPSC MJ2136	w.t.	M	unk.	Sendai	X$	X			X		
iPSC 010198-01-SV-005WT	w.t.	M	68	Sendai*	X$						
iPSC 010198-01-SV-005	PD	M	68	Sendai	X$						
iPSC 010198-01-SV-004	PD	M	68	Sendai	X$	X					
iPSC 050412-01-MR-025	PD	M	63	Aut. mRNA	X$						
iPSC 060102-01-MR-001	MS	M	56	Man. mRNA	X$	X#				X	X
iPSC 050948-01-MR-028	AD	F	40	Aut. mRNA	X$				X	X	X$
hMG	unk.	unk.	fetal	N/A	N/A	X$	X#$	X#	X#	X#	X
hMG-SF	unk.	unk.	fetal	N/A	N/A	X	X#$	X#	X#	X#	X
PB-M(-)	unk.	unk	adult	N/A	N/A	X	X#$	X#	X#	X#	X
PB-M(INFγ,LPS)	unk.	unk.	adult	N/A	N/A	X	X#$	X#	X	X$	X
PB-M(IL4,IL13)	unk.	unk.	adult	N/A	N/A	X	X#$	X#	X	X$	X
PB-M(IL-10)	unk.	unk.	adult	N/A	N/A	X	X#$	X#	X	X$	X

Table S3. Demographic information and specific assay performed for every line described in this manuscript. Related to Experimental Procedures. Table summarizing demographic information, reprogramming method and specific assays performed with each line. "MG Markers" column includes data from flow cytometry and immunofluorescence. MG: Microglial, unk.: unknown, N/A: not applicable, Aut. mRNA: Automated mRNA/miRNA method, Man. mRNA: Manual mRNA/miRNA method. *CRISPR/Cas9 corrected PD line, #Data shown in a main figures, $Data shown in supplemental items.

Supplemental Experimental Procedures

All incubations were performed in a 37°C incubator with 5% CO_2 and all growth factors are human recombinant proteins purchased from R&D Systems, unless otherwise stated. All media contain 1X Penicillin/Streptomycin (P/S) or 1X Antibiotic-Antimycotic (Life Technologies). RT: room temperature.

Detailed information on pluripotent stem cell lines and culture conditions

RUES1 and H9 are NIH approved human ESC lines. All iPSC lines were derived from skin biopsies of de-identified donors upon specific institutional review board approvals and informed consent. The control iPSC lines 050643-01-MR-145 (25 y.o. male), 050652-01-MR-001 (45 y.o. female), 050598-01-MR-025 (53 y.o. male), 051024-01-MR-005 (29 y.o. male), 050689-01-MR-012 (27 y.o. male), 050675-01-MR-012 (34 y.o. male), 050642-01-MR-001 (69 y.o. male), the PD line 050412-01-MR-025 (63 y.o. male) and the AD line 050948-01-MR-028 (40 y.o. female) were reprogrammed using the NYSCF global stem cell array with the mRNA/miRNA method (StemGent) (Paull et al., 2015). 060102-01-MR-001 (56 y.o. male) was reprogrammed manually from a primary progressive multiple sclerosis patient, using mRNA/miRNA (Douvaras et al., 2014). 010198-01-SV-004 and 010198-01-SV-005 are two distinct clones reprogrammed with Sendai virus from a PD patient (68 y.o. male) with a GBA N370S mutation (Woodard et al., 2014) whereas 010198-01-SV-005WT is a CRISPR/Cas9 corrected line (unpublished; kind gift from Dr. Aiqun Li). MJ2136 was a kind gift from Dr. Ricardo Feldman and was reprogrammed with Sendai virus from a healthy control (Panicker et al., 2014).

The human primary microglia and hepatic macrophages were purchased from ScienCell along with Microglia Medium and Macrophage Medium (ScienCell).

PSC lines were cultured and expanded onto Matrigel-coated dishes in mTeSR1 medium (StemCell Technologies). Lines were passaged every 3-4 days using enzymatic detachment with Stempro Accutase (Life Technologies) for 5 min and re-plated in mTeSR1 medium with 10μM Rock Inhibitor (Y2732, Stemgent) for 24 hours.

Isolation of myeloid progenitors

Cells from the supernatant fraction of the cultures were incubated with CX3CR1 and/or CD14 conjugated primary antibodies (see antibody table) or their respective isotype controls for 40 min on ice. Cells were then washed in FACS buffer (PBS, 0.5% BSA, 2mM EDTA, 20mM Glucose), pelleted at 300g for 6 min and resuspended in FACS buffer containing DAPI for dead cell exclusion. $CD14^+$ or $CD14^+CX3CR1^+$ cells were isolated via FACS on an ARIA-IIu™ Cell Sorter (BD Biosciences) using the 100μm ceramic nozzle, and 20 psi.

Freezing and thawing of the myeloid progenitors

Myeloid progenitor cells were frozen after isolation in cryogenic vials (Thermo Scientific) in freezing medium consisting of 90% FBS (Life Technologies) and 10% DMSO (Sigma-Aldrich). Cells were then transferred into a Mr.Frosty (Thermo Scientific) container and placed overnight at -80°C. The next day, cryogenic vials were transferred to liquid nitrogen for long-term storage.

To thaw the cells, the cryogenic vial was transferred in a 37°C water bath for 1-2 min, until partially thawed. Under a laminar flow hood, RPMI-1640 medium was added to 5X the original volume of the vial. Cell were then centrifuged at 300g for 6 min, resuspended in the appropriate amount of medium and plated onto tissue culture treated plastic.

Detailed microglial differentiation protocol

PSCs were plated onto Matrigel (BD Biosciences) in a $15x10^3$ cells/cm^2 density in mTeSR1 medium containing 10μM Rock Inhibitor for 24 hours. When individual colonies were visible (usually 2-4 days after plating), differentiation was induced by providing mTeSR Custom medium (StemCell Technologies), containing 80ng/ml BMP4. mTeSR Custom medium is mTeSR1 medium without Lithium Chloride, GABA, Pipecolic Acid, bFGF and TGFβ1 (Stem Cell Technologies). The medium was changed daily for 4 days, when cells were induced with StemPro-34 SFM (containing 2mM GutaMAX-I, Life Technologies) supplemented with 25ng/ml bFGF, 100ng/ml SCF and 80ng/ml VEGF. Two days later, the medium was switched to StemPro-34 containing 50ng/ml SCF, 50ng/ml IL-3, 5ng/ml TPO, 50ng/ml M-CSF and 50ng/ml Flt3 ligand. On day 10, the supernatant fraction of the cultures was pelleted, resuspended in fresh medium (same as before) and returned to their dishes. On day 14, floating cells were pelleted, resuspended in StemPro-34 containing 50ng/ml M-CSF, 50ng/ml Flt3 ligand and 25ng/ml GM-CSF and replated back to their dishes. The procedure was repeated every four days. From day 24 – 52, a small amount of floating cells was processed for flow cytometry analysis to determine the peak of the CD14/CX3CR1 double positive progenitors. After the isolation of $CD14^+$ or $CD14^+CX3CR1^+$ progenitors, cells were plated onto tissue culture-treated dishes or Thermanox plastic coverslips (all from Thermo Scientific) in a 40-

$50x10^3$ cells/cm^2 in SF–Microglial Medium (RPMI-1640 from Life Technologies supplemented with 2mM GlutaMAX-I, 10ng/ml GM-CSF and 100ng/ml IL-34). Medium was replenished every 3 to 4 days for at least 2 weeks.

Peripheral blood derived macrophages and polarization

Macrophages were differentiated from isolated human mononuclear cells obtained from peripheral blood of healthy individuals at the New York Blood Center as previously described (Pallotta et al., 2015). Briefly, $CD14^+$ cells were isolated after Ficoll gradient and magnetic beads based separation using the EasySep Human CD14 Positive Selection Kit (STEMCELL Technologies). Cells were then seeded in ultra-low attachment plates for 5 days in a $5x10^5$ cells/ml density and differentiated to macrophages using RPMI-1640 supplemented with 2mM GlutaMAX-I, 10% heat-inactivated human serum (Sigma-Aldrich) and 20ng/ml M-CSF (PeproTech). For polarization, macrophages were kept in the same medium (M(-)), or treated for 48 hours with 100ng/ml LPS (Sigma-Aldrich) and 100ng/ml IFNγ (M(LPS, IFNγ)), 40ng/ml IL-4 and 20ng/ml IL-13 (M(IL4,IL13)) or 40ng/ml IL-10 (M(IL10); all from PeproTech).

Immunofluorescent staining

Cells were washed 3X in PBS-T (PBS containing 0.1% Triton-X100) for 10 min, incubated for 2 hours in blocking serum (PBS-T with 5% donkey serum) and primary antibodies (see Antibody Table) were applied overnight at 4°C. The next day, cells were washed 3X in PBS-T for 15 min, incubated with secondary antibodies for 2 hours at room-temperature (RT), washed 3X for 10 min in PBS-T, counterstained with DAPI for 15 min at RT and washed 2X in PBS. Secondary antibodies were used at 1:500 dilution. Images were acquired using an Olympus IX71 inverted microscope, equipped with Olympus DP30BW black and white digital camera. Fluorescent colors were digitally applied using the Olympus software DP Manager or imageJ.

Flow cytometry analysis

Cells were enzymatically harvested by Accutase treatment for 5 min at 37°C and then scrapped with a cell lifter (Sigma-Aldrich). Cells were then re-suspended in 100µl of their respective medium containing the appropriate amount of fluorescence-conjugated antibodies (see Antibody Table) and were incubated on ice for 40 min shielded from light. Isotype controls or secondary antibodies only were used to measure the baseline background signal. DAPI or Sytox Green (Thermofisher) were used for dead cell exclusion. Analyses were performed on a five-laser BD Biosciences ARIA-IIu™ Cell Sorter or on a four-laser Attune NxT Flow Cytometer (ThermoFisher). Data were analyzed using BD FACSDiva™ software or FlowJo version 9.9.4 (FlowJo LLC).

Antibody Table. List of Antibodies used for flow cytometry and immunofluorescent analyses

Name	Host	Vendor	Cat. No.
IBA1	Rabbit	Wako	019-19741
P2RY12	Rabbit	Alomone Labs	APR-020
CD11b-Alexa700	Mouse	BD Pharmingen	557918
CD11c-PE	Mouse	BD Pharmingen	555392
CX3CR1-PE	Mouse	R&D Systems	FAB5204P
CD14-APC	Mouse	BioRad	MCA596APCT
CD45-v450	Mouse	BD Horizon	560367
CD309-APC	Mouse	Miltenyi Biotec	130-093-601
CD235a-PE	Mouse	BD Pharmingen	555570
anti-rabbit IgG-Alexa488	Donkey	ThermoFisher Scientific	A-21206
anti-mouse IgG-Alexa555	Donkey	ThermoFisher Scientific	A-31570

Phagocytosis assay

Phagocytosis assay was performed as previously described (Enomoto et al., 2013). Briefly, Fluoresbrite YG Carboxylate Microspheres 1.00µm (Polysciences) were added to the dishes containing adherent microglial cells in a 200 microspheres/cell ratio. After incubating the cultures at 37^{o}C for 3 hours, fluorescent images were acquired with an Olympus IX71 inverted microscope, equipped with Olympus DP30BW black and white digital camera. Then cells were washed 3X with PBS, treated with Accutase for 5 min and completely detached using a cell lifter. After centrifuging, cells were resuspended in FACS buffer containing DAPI and analyzed on a BD Biosciences ARIA-IIu™ Cell Sorter.

Cytokine Profiler and clustering

For analysis of the secreted cytokine profile of microglial cells, the Human XL Cytokine Array Kit of the Proteome Profiler Antibody Arrays (R&D Systems) was used according to the manufacturer's instructions. Supernatant was collected from the cultures and stored at -80^{o}C for up to 3 months. Membranes were directly visualized in a Kodak Image Station 4000MM PRO and images were acquired using the Carestream Molecular Imaging Software.

For analysis of the signals, images were imported to Image J and the Protein Array Analyzer plugin was used. The intensity reading of the two identical spots was then averaged and the mean value of 8 negative controls was subtracted from every value. Finally, data were expressed as intensity ratio compared to the mean intensity of the 6 reference spots (positive controls). Heatmap and clustering for the protein profiler analysis was generated using heatmap.2 in R version 3.3.1.

Intracellular Ca^{2+} imaging

Cells were cultured onto Thermanox plastic coverslips (ThermoFisher) and were incubated for 30min at 37°C with medium supplemented with the fluorescent Ca^{2+} dye Fluo-4/AM (2mM) mixed at 1:1 with Pluronic-127 reagent (both from Invitrogen). Cells were subsequently washed twice with RPMI-1640 media containing 1% BSA (Life Technologies), 1X GlutaMAX-I and 10mM HEPES (Sigma-Aldrich) pH adjusted to 7.5. Cells were allowed to recover for an additional 30 min to ensure dye esterification. Coverslips were then transferred to a recording chamber mounted onto an upright Olympus BX61 microscope. Fluorescence was recorded at 2Hz by a cooled CCD camera (Hamamatsu Orca R^2). Drug application was done via whole chamber perfusion at room temperature for a period of 60s. $[Ca^{2+}]_i$ transients are expressed in the form of $\Delta F(t)/F_0$, where F_0 is a baseline fluorescence of a given region of interest and ΔF is the difference between current level of fluorescence F(t) and F_0. Fluctuations of $\Delta F(t)/F_0$ that were less than 0.05 were considered as non-responses.

RNA sequencing and analyses

RNA isolation was performed using the RNeasy Plus Mini Kit (Qiagen) with QIAshredder (Qiagen). Cells were enzymatically detached after treatment with Accutase for 5 min and using a cell lifter. After centrifuging, cells were washed with PBS and resuspended in lysis buffer. Samples were then stored at -80^{o}C until processed further according to manufacturer's instructions. RNA was eluted in 30µl RNase free ddH2O and quantified with a NanoDrop 8000 spectrophotometer (Thermo Scientific).

Single-ended RNAseq data were generated with the Illumina HiSeq 2500 platform following the Illumina protocol. The raw sequencing reads were aligned to human hg19 genome using star aligner (version 2.5.0b). Following read alignment, featureCounts (Liao et al., 2014) was used to quantify the gene expression at the gene level based on Ensembl gene model GRCh37.70. Genes with at least 1 count per million (CPM) in at least one sample were considered expressed and hence retained for further analysis, otherwise removed. The gene level read counts data were normalized using trimmed mean of M-values normalization (TMM) method (Robinson et al., 2010) to adjust for sequencing library size difference. Hierarchical cluster analysis based on transcriptome-wide gene expression was performed using R programming language. The RNA sequencing data have been deposited in NCBI's Gene Expression Omnibus and are accessible through GEO Series accession number GSE97744.

For re-analysis of microglia RNAseq data from Zhang et al. (Zhang et al., 2016), we downloaded the raw RNAseq data of "myeloid" cells from gene expression omnibus (GEO: accession GSE73721). The RNAseq read data was processed using the same star/featureCounts pipeline as described above and then the gene level read counts were combined with the gene count data of our samples. The merged data were normalized with the TMM approach and then corrected for batch using linear regression. Hierarchical cluster analysis was used to illustrate the sample dissimilarity.

Similarly, for comparison with a recently published human iPSC-derived microglial dataset from Muffat et al., 2016, we downloaded their RNAseq read data from GEO (accession GSE85839) and then applied the same RNAseq analysis pipeline to obtain gene level count data which was merged with the read count of the present samples. The merged data was normalized and batch corrected before carrying out hierarchical cluster analysis.

Statistics

Frequencies were calculated in excel and expressed as Mean ± Standard Error of the Mean (SEM).

Statistical analysis of $[Ca^{2+}]_i$ transients amplitude was performed using unpaired Student's t-test to compare mean values in excel.

The P value significance of the cluster partition for the dendrogram based on the six signature genes was estimated as the fraction of 1000 repeated permutations (shuffling gene expression values within each gene) in which the cluster center distance obtained from k-means cluster with two centers was more extreme than that in the original data.

Pearson's correlation coefficient between iPSC-MG and hMG or hMG-SF for cytokine release data was calculated using GraphPad Prism 6.

Supplemental References

Douvaras, P., Wang, J., Zimmer, M., Hanchuk, S., O'Bara, M.A., Sadiq, S., Sim, F.J., Goldman, J., and Fossati, V. (2014). Efficient generation of myelinating oligodendrocytes from primary progressive multiple sclerosis patients by induced pluripotent stem cells. Stem cell reports *3*, 250-259.

Enomoto, R., Imamori, M., Seon, A., Yoshida, K., Furue, A., Tsuruda, H., and Lee-Hiraiwa, E. (2013). Proposal for a new evaluation of phagocytosis using different sizes of fluorescent polystyrene microspheres. Advances in Biological Chemistry *03*, 556-563.

Liao, Y., Smyth, G.K., and Shi, W. (2014). featureCounts: an efficient general purpose program for assigning sequence reads to genomic features. Bioinformatics *30*, 923-930.

Pallotta, I., Sun, B., Wrona, E.A., and Freytes, D.O. (2015). BMP protein-mediated crosstalk between inflammatory cells and human pluripotent stem cell-derived cardiomyocytes. Journal of tissue engineering and regenerative medicine.

Panicker, L.M., Miller, D., Awad, O., Bose, V., Lun, Y., Park, T.S., Zambidis, E.T., Sgambato, J.A., and Feldman, R.A. (2014). Gaucher iPSC-derived macrophages produce elevated levels of inflammatory mediators and serve as a new platform for therapeutic development. Stem cells *32*, 2338-2349.

Paull, D., Sevilla, A., Zhou, H., Hahn, A.K., Kim, H., Napolitano, C., Tsankov, A., Shang, L., Krumholz, K., Jagadeesan, P*., et al.* (2015). Automated, high-throughput derivation, characterization and differentiation of induced pluripotent stem cells. Nature methods *12*, 885-892.

Robinson, M.D., McCarthy, D.J., and Smyth, G.K. (2010). edgeR: a Bioconductor package for differential expression analysis of digital gene expression data. Bioinformatics *26*, 139-140.

Woodard, C.M., Campos, B.A., Kuo, S.H., Nirenberg, M.J., Nestor, M.W., Zimmer, M., Mosharov, E.V., Sulzer, D., Zhou, H., Paull, D*., et al.* (2014). iPSC-derived dopamine neurons reveal differences between monozygotic twins discordant for Parkinson's disease. Cell reports *9*, 1173-1182.